JOURNAL OF AGRICULTURAL AND FOOD CHEMISTRY

pubs.acs.org/JAFC Article

# Millet Bran Protein Hydrolysate Displays the Anti-non-alcoholic Fatty Liver Disease Effect via Activating Peroxisome Proliferator-Activated Receptor γ to Restrain Fatty Acid Uptake

Shuhua Shan,*,† Jiaqi Zhou,† Ruopeng Yin, Lizhen Zhang, Jiangying Shi, Qinqin Qiao, and Zhuoyu Li*

Cite This: J. Agric. Food Chem. 2023, 71, 1628−1642 Read Online

ACCESS | Metrics & More | Article Recommendations | Supporting Information

**ABSTRACT:** Non-alcoholic fatty liver disease (NAFLD) is a serious health problem worldwide. Impeding fatty acid uptake may be an attractive therapeutic strategy for NAFLD. In the current study, we found that millet bran protein hydrolysate (MBPH) prepared by *in vitro* gastrointestinal bionic digestion exhibits the potential of anti-NAFLD *in vitro* and *in vivo*, characterized by the alleviation of hepatic steatosis and the reduction of lipid accumulation. Further, MBPH significantly decreased the expression levels of fatty acid uptake related genes (FABP1, FABP2, FABP4, CD36, and CPT-1α) of liver tissue in a NAFLD mice model through activating peroxisome proliferator-activated receptor γ (PPARγ) and efficiently restrained the fatty acid uptake of liver tissue, thus exerting anti-NAFLD activity. As expected, the anti-NAFLD effect induced by MBPH, characterized by the alleviation of hepatic vacuolar degeneration, hepatic steatosis, and fibrosis, was effectively abrogated with PPARγ inhibitor (GW9662) treatment. These results indicate that the retardant of fatty acid uptake induced by PPARγ activation may be the critical factor for the anti-NAFLD effect of MBPH. Collectively, MBPH has the potential as a next-generation dietary supplementation for the prevention and treatment of NAFLD.

**KEYWORDS:** *millet bran protein hydrolysate, PPARγ, fatty acid uptake, NAFLD*



## INTRODUCTION

Currently, non-alcoholic fatty liver disease (NAFLD) has been the most common liver disease worldwide that combined with complex exacerbating symptoms, such as liver fibrosis and cancer, which has become a surging burden as a result of its high prevalence. Currently, there are still no effective drugs for the treatment of NAFLD.[1] Most patients with NAFLD are clinically asymptomatic, and few patients can present with symptoms of fatigue, dyspepsia, dull liver pain, and hepatosplenomegaly.[2] Therefore, the development of functional foods and effective drugs against NAFLD is imminent. NAFLD is characterized by hepatic steatosis. In NAFLD, hepatic lipid uptake or *de novo* lipogenesis is abnormally increased, but compensatory enhancement of fatty acid oxidation is insufficient to normalize lipid levels, which promotes lipid accumulation and even leads to cellular damage and NAFLD progression.[3] NAFLD driven by systemic metabolic disorders is closely related to metabolic syndrome diseases, such as hyperglycemia, insulin resistance, and obesity. Inhibition of lipid uptake can be a target for the prevention and control of NAFLD. Many natural products have been reported to exert efficacy in alleviating NAFLD by modulating lipid metabolism disorder.[4] Therefore, searching for active molecules against NAFLD from natural products is an attractive therapeutic strategy.

The multiple functions of plant protein hydrolysates have great potential in food and health. The study has elucidated that rice bran protein and its hydrolysates have better health care effects, including antioxidant, antihypertensive, antidiabetic, cholesterol-lowering, and anticancer activities.[5] 3-Hydroxy-3-methylglutaryl CoA reductase (HMGCoAR) is the key rate-limiting enzyme in the mevalonate pathway for cholesterol biosynthesis.[6] Ashraf et al. demonstrated that adzuki protein and faba protein hydrolysates by simulated human digestion exhibited the HMGCoAR inhibitor activity, suggesting that they may play an important role in lowering the cholesterol effect.[7] Alashi et al. found that canola protein and its enzymatic hydrolysates display a specific antiobesity effect via regulating the differentiation of adipocytes *in vitro*.[8] Hence, these studies indicate that plant-derived protein hydrolysates have potential promising applications in alleviating chronic diseases.

Evidence from epidemiological and clinical studies indicate the improved glycaemic control in patients with diabetes who consume whole grains as well as increased insulin sensitivity in non-diabetic individuals who consume large amounts of whole-grain foods,[9−11] suggesting that the increased intake of whole grains can alleviate NAFLD. The study by Murtaza et al. showed that 10% (w/w) millet bran could prevent weight gain, improve lipid status, and regulate the expression levels of several obesity-related genes of high-fat diet (HFD)-induced mice.[12] Hence, whole grain intake may open a new avenue for anti-NAFLD. The studies indicate that peptides derived from grains have the potential for medicinal development in the treatment of

Received: November 21, 2022
Revised: December 24, 2022
Accepted: December 27, 2022
Published: January 13, 2023

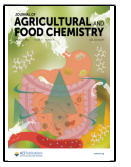





https://doi.org/10.1021/acs.jafc.2c08169
J. Agric. Food Chem. 2023, 71, 1628−1642

NAFLD.[13] For example, the research of Ipsen et al. showed that grain proteins have the efficacy of improving lipid metabolism disorder and alleviating liver injury.[1] Nishizawa et al. found that grain proteins exhibited a significant antiatherogenic effect through increasing the plasma concentrations of high-density lipoprotein (HDL).[14] The research of Ofosu et al. showed that the active peptides derived from cereal can alleviate metabolic syndrome, such as type 2 diabetes, obesity, hypertension, cardiovascular diseases, and certain cancers.[15] Therefore, the increasing intake of whole grains in the diet may be an effective strategy for prevention and treatment of NAFLD.

Millet bran is a byproduct during the processing of millet. The essential amino acid content of millet bran protein is 41.2%, which has a high nutritional value. Studies have shown that millet bran protein is the least allergenic protein of the grains known and is suitable for dietary supplement of sub-healthy people.[16] Recent studies have discovered that millet bran contains a series of active proteins and peptides with medicinal values, which exhibit multiple efficacies, such as remodeling gut microbiota, antiatherosclerosis,[17] and antitumor.[18] In the present study, we found that millet bran protein hydrolysate (MBPH) prepared by *in vitro* gastrointestinal bionic digestion exhibited the potential of anti-NAFLD activity *in vitro* and *in vivo*. Further, peroxisome proliferator-activated receptor $\gamma$ (PPAR$\gamma$) activation-induced retardant of fatty acid uptake may be the critical factor for the anti-NAFLD activity of MBPH. The highlight of this study lies in the discovery of a new pharmacological function of MBPH in anti-NAFLD activity, which is expected to be the next-generation dietary supplementation for the prevention and treatment of NAFLD.

## MATERIALS AND METHODS

**Reagents and Antibodies.** NAFLD-inducing agent oleic and palmitic acids were purchased from Sigma (St. Louis, MO, U.S.A.). RPMI-1640 medium and fetal bovine serum (FBS) was purchased from GIBCO (Grand Island, NY, U.S.A.). Oil red O lipid stain kit, penicillin−streptomycin−gentamycin mixed solution, trilaurin, and antifade mounting medium were purchased from Solarbio (Beijing, China). The screen quest fluorimetric fatty acid uptake assay kit was purchased from AAT Bioquest (Pleasanton, CA, U.S.A.). Trypsin and pepsin were purchased from Sigma (St. Louis, MO, U.S.A.). Sodium dodecyl sulfate (SDS), 3-(4,5-dimethylthiazol-2-yl)-2,5-diphenyltetrazolium bromide (MTT), and dimethyl sulfoxide (DMSO) were obtained from Sigma (St. Louis, MO, U.S.A.). GW9662 was obtained from MedChemExpress (Shanghai, China). BODIPY was purchased from ChemeGen (Shanghai, China). The thin-layer chromatography silica gel plate was purchased from Yantai Jangyou Silica Gel Development Co., Ltd. (Yantai, China). 2,6-Di-*tert*-butyl-4-methylphenol was obtained from Aladdin (Shanghai, China). Iodine was purchased from Macklin (Shanghai, China). Triglyceride (TG, A110-1-1), total cholesterol (T-CHO, A111-1-1), high-density lipoprotein cholesterol (HDL, A112-1-1), low-density lipoprotein cholesterol (LDL, A113-1-1), alanine aminotransferase (ALT, C009-3-1), and aspartate aminotransferase (AST, C010-3-1) assay kits were procured from Nanjing Jiancheng Bioengineering Institute (Nanjing, China). Fatty acid binding protein 4 (FABP4) and glyceraldehyde 3-phosphate dehydrogenase (GAPDH) antibodies were purchased from Bioworld Technology, Inc. (Nanjing, China). The nuclear and cytoplasmic protein extraction kit was purchased from Keygen (Nanjing, China). The bicinchoninic acid (BCA) protein assay kit was procured from Beyotime (Shanghai, China). The antibodies for fatty acid binding protein 1 (FABP1), PPAR$\gamma$, and cluster of differentiation 36 (CD36) were purchased from Proteintech (Wuhan, China). The antibodies for fatty acid binding protein 2 (FABP2) and carnitine palmitoyltransferase 1$\alpha$ (CPT-1$\alpha$) were purchased from Affinity Biosciences (Jiangsu, China). Goat anti-rabbit immunoglobulin G (IgG) heavy and light (H&L)/horseradish peroxidase (HRP) antibody was purchased from Bioss (Beijing, China).

**Bionic Digestion of Millet Bran Protein *in Vitro*.** Bionic digestion of millet bran protein *in vitro* was followed according to our previously described method.[17] Briefly, millet bran protein extract was digested using the pepsin buffer of 250 units/mL (pH 1.6) at 37 °C for 0.5 h away from light, followed by simulated intestinal digestion using the trypsin buffer of 200 units/mL at pH 6.8 (containing 5% $NaHCO_3$) and 37 °C for 1.5 h away from light. Then, the hydrolysate was incubated for 10 min at 80 °C to stop the digestion, followed by centrifugation for 10 min (at 10000*g* and 4 °C). The supernatant was desalted with 100 Da dialysis tubing to obtain the MBPH.

**Cell Culture and Treatment.** For stock solution preparation, 19.23 mg of palmitic acid (PA) and 63.55 $\mu$L of oleic acid (OA) were respectively dissolved in 150 $\mu$L of DMSO to ensure an ultimate concentration of 2 M free fatty acids (FFAs). All stock solutions were deposited at −20 °C. HepG2 cell lines were procured from the Chinese Type Culture Collection (Shanghai, China). HepG2 cells were cultured in the complete medium containing 10% FBS (v/v) under incubator conditions of 5% $CO_2$ at 37 °C. After seeded in 24-well plates to culture for 12 h, HepG2 cells were treated 24 h with a final concentration of 1 mM FFAs to induce a lipid degeneration model, followed by the treatment of 0.3 and 0.6 mg/mL of MBPH for 48 h, respectively.

**Animals and Diets.** A total of 40 male C57BL/6 mice (4 weeks old) were purchased from Charles River (Beijing, China) and fed in the specific pathogen-free (SPF) environment. After 1 week of acclimation, the mice were stochasticly divided into four groups (10 mice/group) to facilitate different interventions. Except for the control group given a normal diet (MolDiets, Beijing, China), the model group, MBPH-L group (50 mg/kg), and MBPH-H group (100 mg/kg) were given a HFD (MolDiets, Beijing, China). In the PPAR$\gamma$ inhibitor intervention experiment, the mice were also stochasticly assigned into four groups with 10 mice in each group. Except for the control group given a normal diet, the model group, MBPH group (100 mg/kg), and GW9662 (1 mg/kg) and MBPH (100 mg/kg) co-treatment group were given a HFD. MBPH and GW9662 were given to mice via intragastric administration. After feeding for 12 weeks, C57BL/6 mice fasted for 24 h. Further, fresh blood was taken for measurement. The liver of mice was removed and processed with 4% paraformaldehyde to become fixed. All animal experiment procedures were reviewed and approved by the Institutional Animal Care and Use Committee of the Laboratory Animal Center, The China Institute for Radiation Protection.

**Oil Red O Staining.** The effect of MBPH on lipid accumulation was measured using the oil red O kit. After washing with phosphate-buffered saline (PBS) 3 times, HepG2 cells were fixed by 4% paraformaldehyde for 30 min, followed by the oil red O staining according to the kit instruction. Then, these stained cells were photographed under an inverted microscope (40× magnification), and quantitative analysis was performed using ImageJ software.

**BODIPY Staining.** BODIPY staining solution was diluted to 2 $\mu$M with PBS in advance. After washing with PBS 3 times, HepG2 cells were fixed with 4% paraformaldehyde for 30 min, followed by staining with BODIPY (2 $\mu$M) solution for 30 min away from light. Next, to discard the staining solution, cells were rinsed with PBS 3 times and stained by 1 $\mu$M 4′,6-diamidino-2-phenylindole (DAPI) solution for 5 min at 37 °C in darkness. After rinsing with PBS 3 times, cells were added antifade mounting medium to avoid fluorescence quenching. These stained cells were photographed under an inverted microscope (100× magnification), and quantitative analysis was performed using ImageJ software.[19]

**Thin-Layer Chromatography for Lipids.** HepG2 cells were suspended with 2 mL of PBS buffer containing protease inhibitor and 1 mM phenylmethylsulfonyl fluoride (PMSF). Then, to the solution was added 4 mL of chloroform/methanol (2:1, v/v) and 0.01% butylated hydroxytoluene to vortex, centrifuging for 5 min at 1500*g*, and the organic phase was collected. The remaining water phase was mixed with 2.5 mL of chloroform and vortexed, followed by centrifugation at 1500*g* for 5 min again and mixing with organic phase. The different groups of organic phases were successively placed on the silica gel plate by capillary points, and hexane/diethyl ether/acetic acid (82:18:1, v/v/v)


https://doi.org/10.1021/acs.jafc.2c08169
J. Agric. Food Chem. 2023, 71, 1628−1642

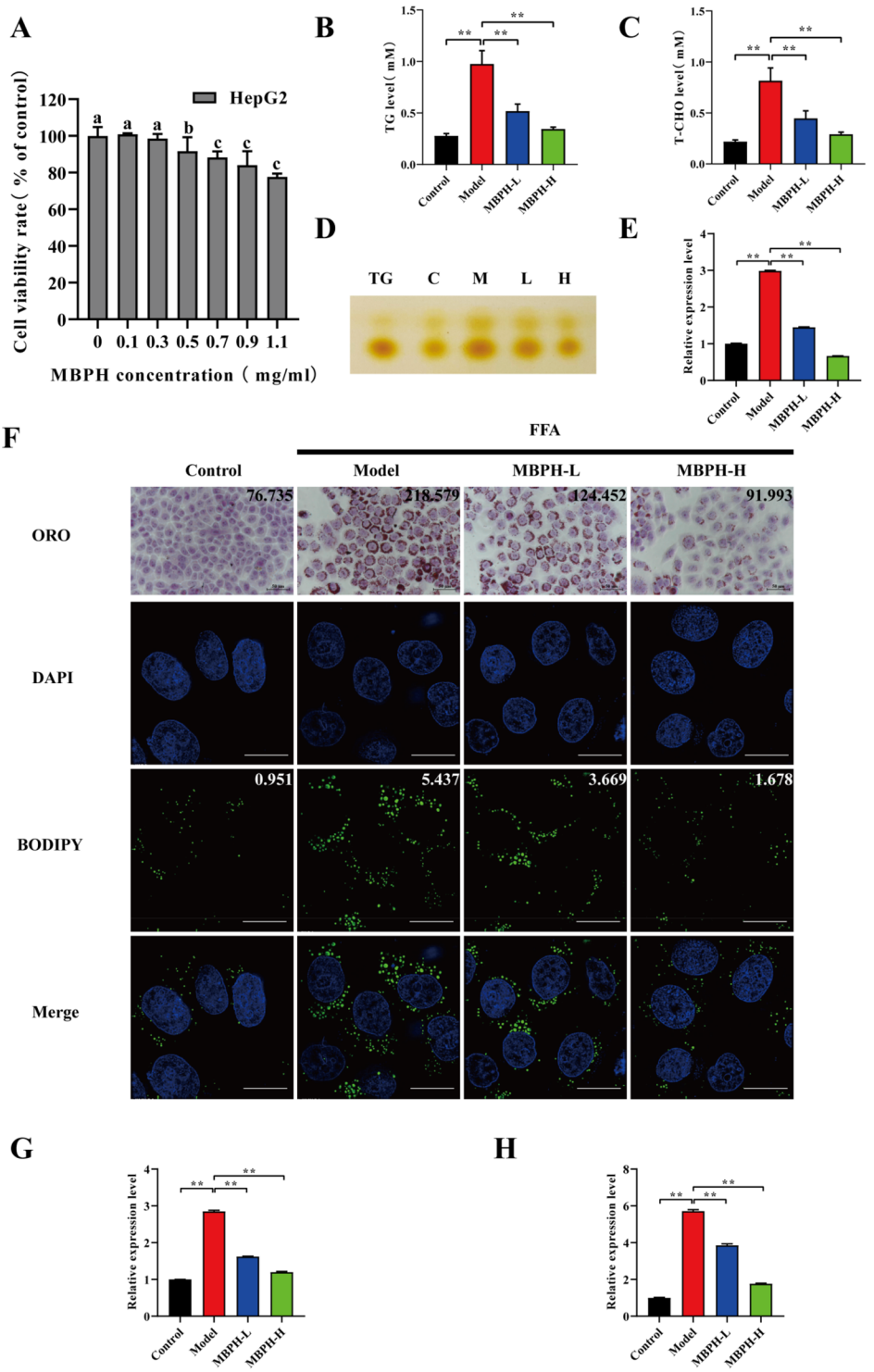


**Figure 1.** MBPH attenuates the lipid accumulation induced by FFAs in HepG2 cells. (A) Effect of MBPH treatment on cell growth. The HepG2 cell was treated for 24 h with different doses (0, 0.1, 0.3, 0.5, 0.7, 0.9, and 1.1 mg/mL) of MBPH, and the cell viability rate was measured by the MTT assay. The columns with different letters between groups represented significant differences. (B) TG levels in the HepG2 cell. Values are expressed as the mean ± SD ($n \geq 3$/group). (*) $p < 0.05$ and (**) $p < 0.01$ compared to the model group. (C) T-CHO levels in the HepG2 cell. Values are expressed as the mean ± SD ($n \geq 3$/group). (*) $p < 0.05$ and (**) $p < 0.01$ compared to the model group. (D) Thin-layer chromatography of total cellular lipids in HepG2 cells. (E) Quantitative analyses of their TG content using ImageJ software. Values are expressed as the mean ± SD ($n \geq 3$/group). (*) $p < 0.05$ and (**) $p < 0.01$ compared to the model group. (F) Lipid accumulation was measured by oil red O staining and BODIPY staining. Scale bar = 50 $\mu$m. (G) Dyeing area in HepG2 cells was analyzed using ImageJ software. Values are expressed as the mean ± SD ($n \geq 3$/group). (*) $p < 0.05$ and (**) $p < 0.01$ compared to the model group. (H) Fluorescent area in HepG2 cells was analyzed using ImageJ software. Values are expressed as the mean ± SD ($n \geq 3$/group). (*) $p < 0.05$ and (**) $p < 0.01$ compared to the model group.



https://doi.org/10.1021/acs.jafc.2c08169
J. Agric. Food Chem. 2023, 71, 1628−1642

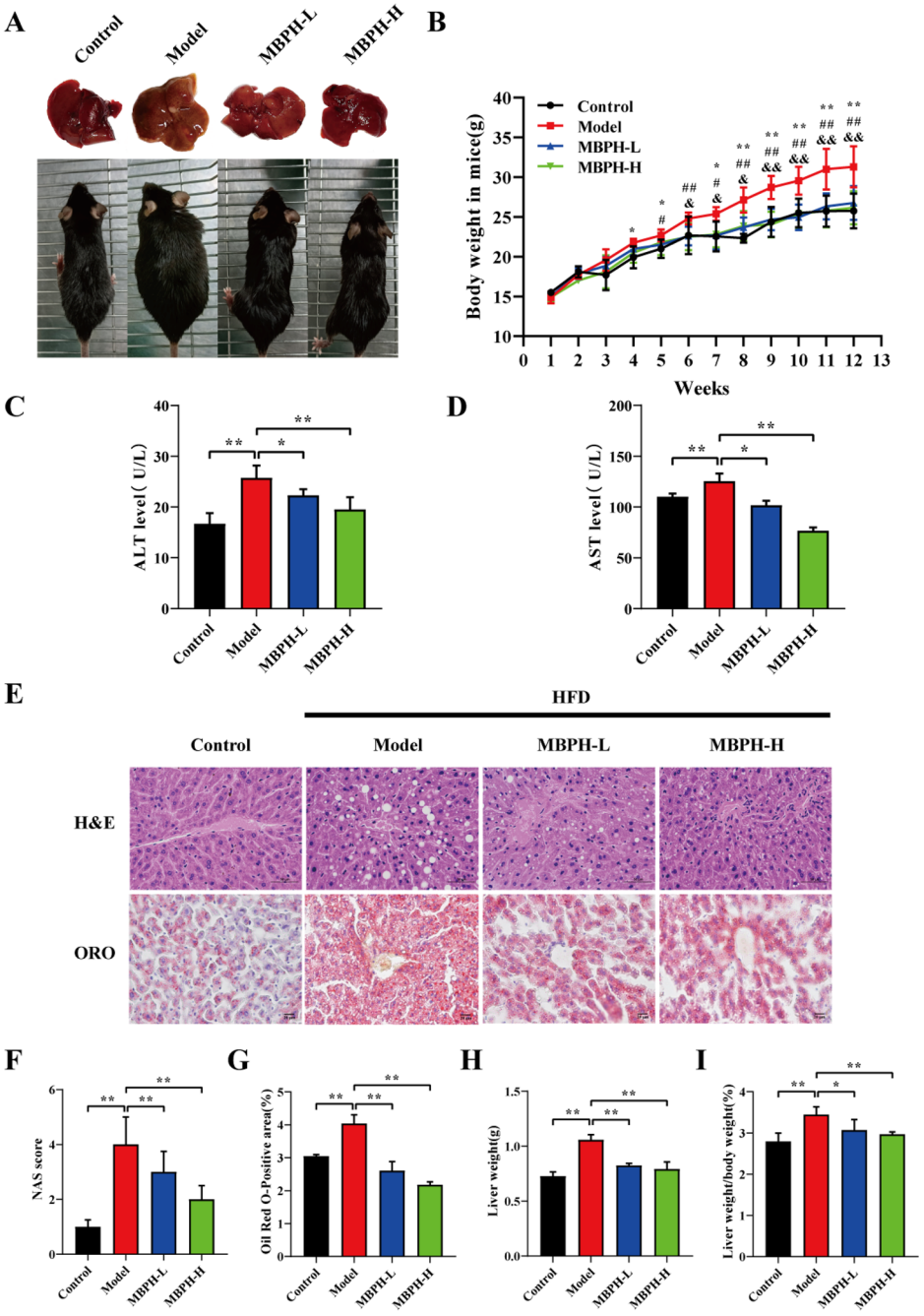


**Figure 2.** MBPH attenuates hepatic steatosis induced by a HFD in mice. (A) Representative photos of the mice and livers. (B) Effect of MBPH in mice fed the HFD on body weight. The weight change of four groups (mean ± SD). The black line marks the control group; the red line marks the model group; the blue line marks the MBPH-L group; and the green line marks the MBPH-H group. Values are expressed as the mean ± SD ($n \geq 6$/group). (∗) $p < 0.05$ and (∗∗) $p < 0.01$ of the control versus model group. (#) $p < 0.05$ and (##) $p < 0.01$ of the model group versus MBPH-L group. (&) $p < 0.05$ and (&&) $p < 0.01$ of the model group versus MBPH-H group. (C) ALT levels in the liver. Values are expressed as the mean ± SD ($n \geq 6$/group). (∗) $p < 0.05$ and (∗∗) $p < 0.01$ compared to the model group. (D) AST levels in the liver. Values are expressed as the mean ± SD ($n \geq 6$/group). (∗) $p < 0.05$ and (∗∗) $p < 0.01$ compared to the model group. (E) Hepatic steatosis and lipid accumulation were measured by H&E and oil red O staining. Scale bar = 50 and 20 $\mu$m. (F) Hepatic steatosis was detected by the NAFLD activity score in the indicated groups. Values are expressed as the mean ± SD ($n \geq 6$/group). (∗) $p < 0.05$ and (∗∗) $p < 0.01$ compared to the model group. (G) Dyeing area in livers was analyzed using ImageJ software. Values are expressed as the mean ± SD ($n \geq 6$/group). (∗) $p < 0.05$ and (∗∗) $p < 0.01$ compared to the model group. (H) Liver weight values of mice. Values are expressed as the mean ± SD ($n \geq 6$/group). (∗) $p < 0.05$ and (∗∗) $p < 0.01$ compared to the model group. (I) Liver weight/body weight values of mice. Values are expressed as the mean ± SD ($n \geq 6$/group). (∗) $p < 0.05$ and (∗∗) $p < 0.01$ compared to the model group.

was used as the developing solvent. Iodine vapor was indicated for visualization of lipids, and quantitative analysis was performed using ImageJ software.[20]

**MTT Assay.** The effect of MBPH on HepG2 cell viability was evaluated using the MTT assay. Cells were seeded in 96-well plates with a density of $6 \times 10^3$ cells per well. After treatment for 48 h with MBPH, each well was added with a final concentration of 5 mg/mL MTT solution and incubated in the cell incubator for 4 h. The absorbance at 570 nm was measured by the microplate reader.



https://doi.org/10.1021/acs.jafc.2c08169
J. Agric. Food Chem. 2023, 71, 1628−1642

**RNA Extraction and Quantitative Polymerase Chain Reaction (qPCR) Assay.** Total RNA in cells and tissues was extracted by Trizol reagent, and the concentration was determined by NanoDrop. According to the instructions of the manufacturer, RNA was reverse-transcribed using HiScript II Q RT SuperMix for qPCR (+gDNA wiper, Vazyme) to obtain the cDNA. Then, real-time qPCR was used to detect mRNA expression using ChamQ Universal SYBR qPCR Master Mix (Vazyme). All primers were designed and synthesized by Sangon Biotech Co., Ltd. (Shanghai, China), and the sequences are shown in Table S1 of the Supporting Information.

**Western Blot Analysis.** Protein concentrations of cells and tissues from different groups were measured by the BCA protein assay kit. Protein samples of different groups with equivalent amounts were separated using 10% sodium dodecyl sulfate polyacrylamide gel electrophoresis (SDS−PAGE) gels and then transferred to polyvinylidene fluoride (PVDF) membranes. The PVDF membranes were blocked using 5% skim milk, followed by incubation successively with primary antibodies at 4 °C for 12 h and HRP-conjugated secondary antibodies at room temperature for 2 h. At the end of incubation, PVDF membranes was washed with 1× Tris-buffered saline with Tween 20 (TBST) buffer 3 times. Protein bands were visualized using Basis ECL Prime (Seven Biotech). GAPDH or proliferating cell nuclear antigen (PCNA) were used as controls.

**Nuclear and Cytoplasmic Protein Extraction.** The protein extraction was performed using the nuclear and cytoplasmic protein extraction kit. HepG2 cells were washed 3 times with PBS, followed by the protein extraction of nuclear and cytoplasmic protein according to the kit instructions. The protein concentration was detected using the BCA protein assay kit.

**NAFLD Activity Score.** The NAFLD activity score is the sum of the scores for steatosis (0−1), hydropic degeneration (0−1), inflammatory cell infiltration (0−1), and necrosis (0−1). A score of 0 is considered to be within the normal range; 0−1 indicates that changes have just exceeded the normal range; 1−2 indicates that the lesion is observable but not severe; 2−3 indicates that the lesion is significant and probably more severe; and 3−4 indicates that the lesion is very severe and has taken over the entire tissue.

**Transcriptome Analysis.** The transcriptome sequencing service of liver tissues of mice was provided by BioTree (Shanghai, China). The mRNA in the liver samples of mice in different groups was enriched separately by poly-T magnetic beads. According to the instructions of the manufacturer, sequencing libraries were constructed by the NEBNext Ultra RNA library preparation kit (NEB, Ipswich, MA, U.S.A.) and sequenced with the NovaSeq 6000 system. Differential analyses between liver samples from different groups were performed by DESeq2 (version 1.28.1). The reference sequences were from Gencode (version M24), and the statistical significance of sequencing results was tested by the multivariate analysis of variance (MANOVA) test.

**Liquid Chromatography−Tandem Mass Spectrometry (LC−MS/MS) Analysis.** LC−MS/MS analysis was provided by Bioprofile (Shanghai, China). The experiment was performed on the Easy nLC (Thermo Scientific). Mobile phase A was 0.1% formic acid aqueous solution, and mobile phase B consisted of a mixture of 0.1% formic acid, acetonitrile, and water, in which acetonitrile accounted for 80%. The gradient was as follows: 0−2 min, 3−5% B; 2−42 min, 5−25% B; 42−52 min, 25−45% B; 52−55 min, 45−90% B; and 55−75 min, 90% B, at the flow rate of 300 nL/min. Parameter settings were referred to the instructions of the manufacturer. Peptides were analyzed by data-dependent acquisition (DDA) mass spectrometry on a Q-Exactive Plus mass spectrometer (Thermo Scientific).

**Histopathology and Immunohistochemistry Assays.** Liver samples of mice were fixed using 4% paraformaldehyde for 24 h and embedded in paraffin, followed by staining with hematoxylin and eosin (H&E), oil red O, and picrosirius red according to the instructions of the manufacturer, respectively, to observe the histological characteristics of liver tissues of mice. The expression level of PPAR$\gamma$ in liver tissues of mice were observed by the immunohistochemistry assay. The inverted microscope was used to photograph the stained sections, and quantitative analysis was performed using ImageJ software.

**Detection of the FFA Level.** The cell culture medium and mouse serum were collected after MBPH treatment. The FFA content in the different samples was detected with the FFA assay kit according to the instructions of the manufacturer.

**Statistical Analysis.** Data are demonstrated in the mean ± standard deviation (SD) form. The data statistical analysis was performed using Student's $t$ test on SPSS software. (*) $p < 0.05$ and (**) $p < 0.01$ in the results represent significant and extremely significant differences, respectively. All of the experiments were conducted at least 3 times.

## RESULTS

**Anti-NAFLD Effect of MBPH in the Lipid Accumulation Model Induced by FFAs.** NAFLD diagnosis involves the measurement of hepatic steatosis, which is characterized by lipid accumulation in hepatocytes. To investigate whether MBPH could reduce hepatic lipid accumulation *in vitro* to exert the anti-NAFLD effect, HepG2 cells were exposed to FFAs (1 mM) with or without MBPH for 24 h and the contents of TG and T-CHO were measured. By the MTT assay, we found that 0.3 and 0.6 mg/mL MBPH had no significant effect on the survival of HepG2 cells, and the doses were selected for subsequent lipid phagocytosis experiments (Figure 1A). Intracellular levels of TG and T-CHO, which reflect lipid accumulation in cells were significantly upregulated in the model group, while this trend was significantly reversed by MBPH treatment (panels B and C of Figure 1). Thin-layer chromatographic analysis of total lipid content demonstrated that the TG level in the model group was significantly enhanced but the trend was partly reversed by MBPH treatment (panels D and E of Figure 1). As shown by the oil red O staining and BODIPY staining, the lipid accumulation in HepG2 cells was induced by the exposure to FFAs, which was decreased when the cells were treated with MBPH (panels F−H of Figure 1). These results indicate that MBPH can display the anti-NAFLD activity by inhibiting cell lipid accumulation *in vitro*.

**MBPH Exerts the Anti-NAFLD Effect in the Hepatic Steatosis Model Induced by HFD.** To examine the pharmacological effects of MBPH on hepatic steatosis and injury in the NAFLD, the relative indexes of lipid accumulation were determined by a HFD-induced NAFLD mice model. Data from gross anatomy revealed that MBPH treatment markedly alleviated hepatic steatosis in the model mice (Figure 2A). In the beginning, the four groups had no obvious difference in body weight. After 4 weeks, in comparison to the control group, the body weight was significantly increased in the model group ($p < 0.05$). After treatment with MBPH for 6 weeks, the mice showed a significant trend of weight loss ($p < 0.05$). Noteworthy, after 9 weeks, in comparison to the model group, the body weight was decreased in the MBPH-L and MBPH-H groups, reaching an extremely significant level ($p < 0.01$), which indicates that MBPH significantly reduces the HFD-induced weight gain in mice (Figure 2B). As known, ALT and AST are generally important markers in NAFLD. The enzyme-linked immunosorbent assay (ELISA) revealed that the enhanced ALT and AST activities of mice serum in the model group were significantly decreased in the MBPH group (panels C and D of Figure 2). Further, H&E staining and NAFLD activity score (NAS) showed that hepatic vacuolar degeneration induced by lipotoxicity was observed in model mice fed a HFD, which was significantly alleviated in MBPH treatment. In addition, oil red O staining showed that MBPH treatment significantly reduced the hepatic lipid droplet accumulation in the model group (panels E−G of Figure 2). The increased liver weight and liver


https://doi.org/10.1021/acs.jafc.2c08169
J. Agric. Food Chem. 2023, 71, 1628−1642

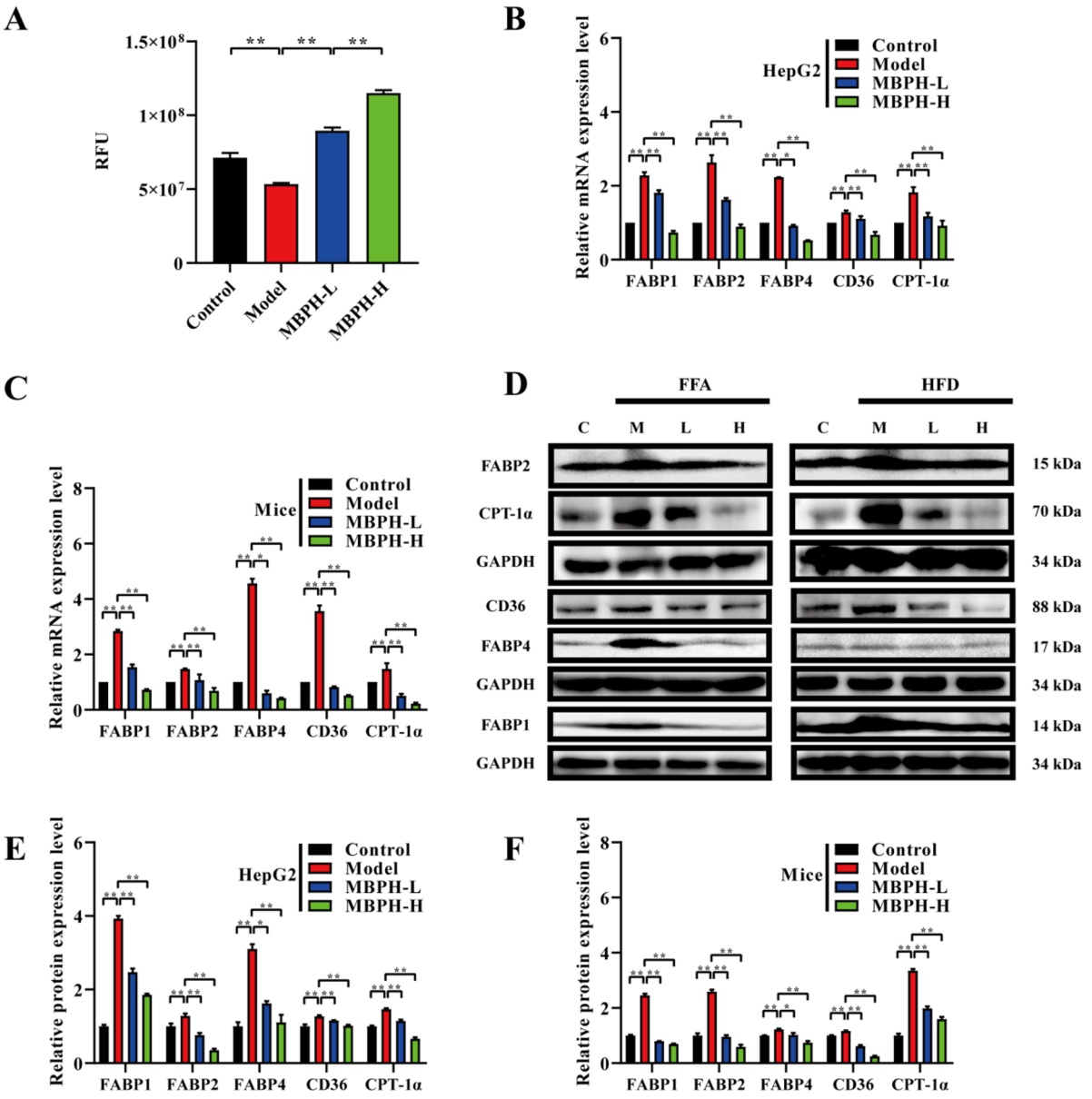


**Figure 3.** MBPH restrains fatty acid uptake *in vivo* and *in vitro*. (A) Fatty acid uptake in the HepG2 cell culture medium in the indicated groups was stimulated with FFAs (1.0 mM) for 24 h. Values are expressed as the mean ± SD ($n \geq 3$/group). (*) $p < 0.05$ and (**) $p < 0.01$ compared to the model group. (B) Quantitative real-time PCR analysis of the transcript levels of genes related to fatty acid uptake (FABP1, FABP2, FABP4, CD36, and CPT-1$\alpha$) *in vitro*. Gene expression was normalized to GAPDH mRNA levels. Values are expressed as the mean ± SD ($n \geq 3$/group). (*) $p < 0.05$ and (**) $p < 0.01$ compared to the model group. (C) Quantitative real-time PCR analysis of the transcript levels of genes related to fatty acid uptake (FABP1, FABP2, FABP4, CD36, and CPT-1$\alpha$) *in vivo*. Gene expression was normalized to GAPDH mRNA levels. Values are expressed as the mean ± SD ($n \geq 6$/group). (*) $p < 0.05$ and (**) $p < 0.01$ compared to the model group. (D) Expression levels of fatty-acid-uptake-related genes (FABP1, FABP2, FABP4, CD36, and CPT-1$\alpha$) were determined *in vivo* and *in vitro* treated with MBPH by western blot assay. GAPDH served as a loading control. (E) Quantitative analysis of the relative protein expression using ImageJ software *in vitro*. Values are expressed as the mean ± SD ($n \geq 3$/group). (*) $p < 0.05$ and (**) $p < 0.01$ compared to the model group. (F) Quantitative analysis of the relative protein expression using ImageJ software *in vivo*. Values are expressed as the mean ± SD ($n \geq 6$/group). (*) $p < 0.05$ and (**) $p < 0.01$ compared to the model group.

weight/body weight ratio in the model group was remarkably decreased by MBPH (panels H and I of Figure 2). Collectively, these data demonstrate that MBPH treatment significantly inhibits the hepatic steatosis in NAFLD model mice, which indicates that MBPH has the potential effect of anti-NAFLD *in vivo*.

**MBPH Impedes the Fatty Acid Uptake *in Vitro* and *in Vivo*.** NAFLD is closely related to fatty acid uptake, and hence, the retardant of fatty acid uptake in the liver may become a new treatment strategy to intervent in NAFLD. The FABP1, FABP2, FABP4, and CD36 are responsible for fatty acid uptake in NAFLD, while CPT-1$\alpha$ is a rate-limiting enzyme regulating the $\beta$-oxidation pathway. Results of FFA content in cell culture medium showed that MBPH treatment significantly increased the content of the FFA in the culture medium compared to the model group, which indicated that MBPH could inhibit fatty acid uptake (Figure 3A). To measure the effect of MBPH on the expression levels of fatty-acid-uptake-related genes of liver tissue in NAFLD mice, qPCR and western blotting assays were carried out. As shown in panels B and C of Figure 3, in comparison to


https://doi.org/10.1021/acs.jafc.2c08169
J. Agric. Food Chem. 2023, 71, 1628−1642

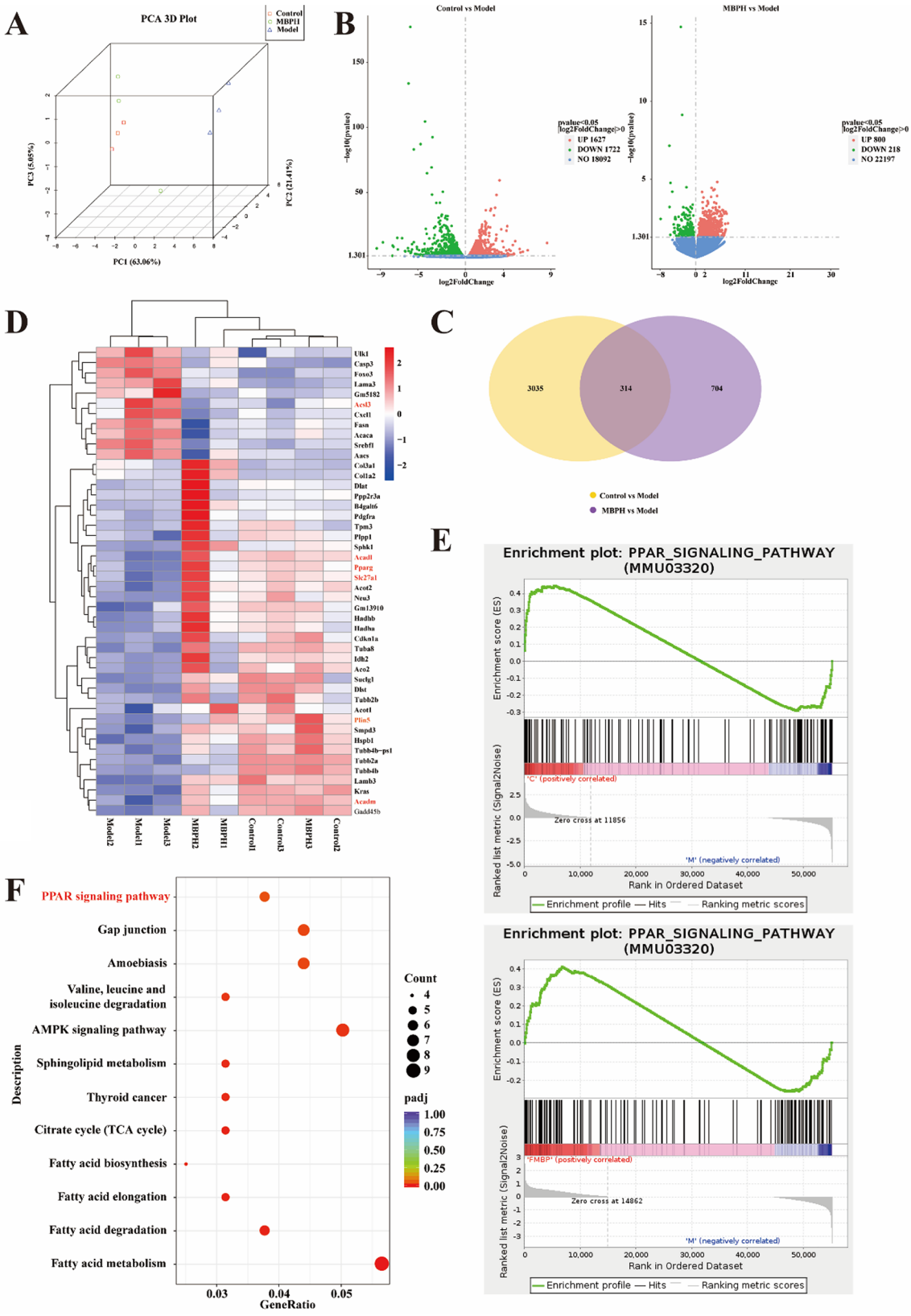


**Figure 4.** Transcriptome analysis of the liver samples in the NAFLD mice. (A) Principal component analysis (PCA). The percent variation explained by each principal coordinate is indicated on the axes. (B) Volcano plots show differentially expressed genes (DEGs). (C) Venn diagram for OTUs. (D) Heat map of the representative DEGs in the indicated groups based on RNA-seq data. (E) Enrichment analysis of the PPAR$\gamma$ signaling pathway. (F) GSEA pathway enrichment analysis.

the model group, the expression levels of FABP1, FABP2, FABP4, CD36, and CPT-1$\alpha$ presented a markedly declining trend in MBPH groups. Similarly, the expression levels of FABP1, FABP2, FABP4, CD36, and CPT-1$\alpha$ were further



https://doi.org/10.1021/acs.jafc.2c08169
J. Agric. Food Chem. 2023, 71, 1628−1642

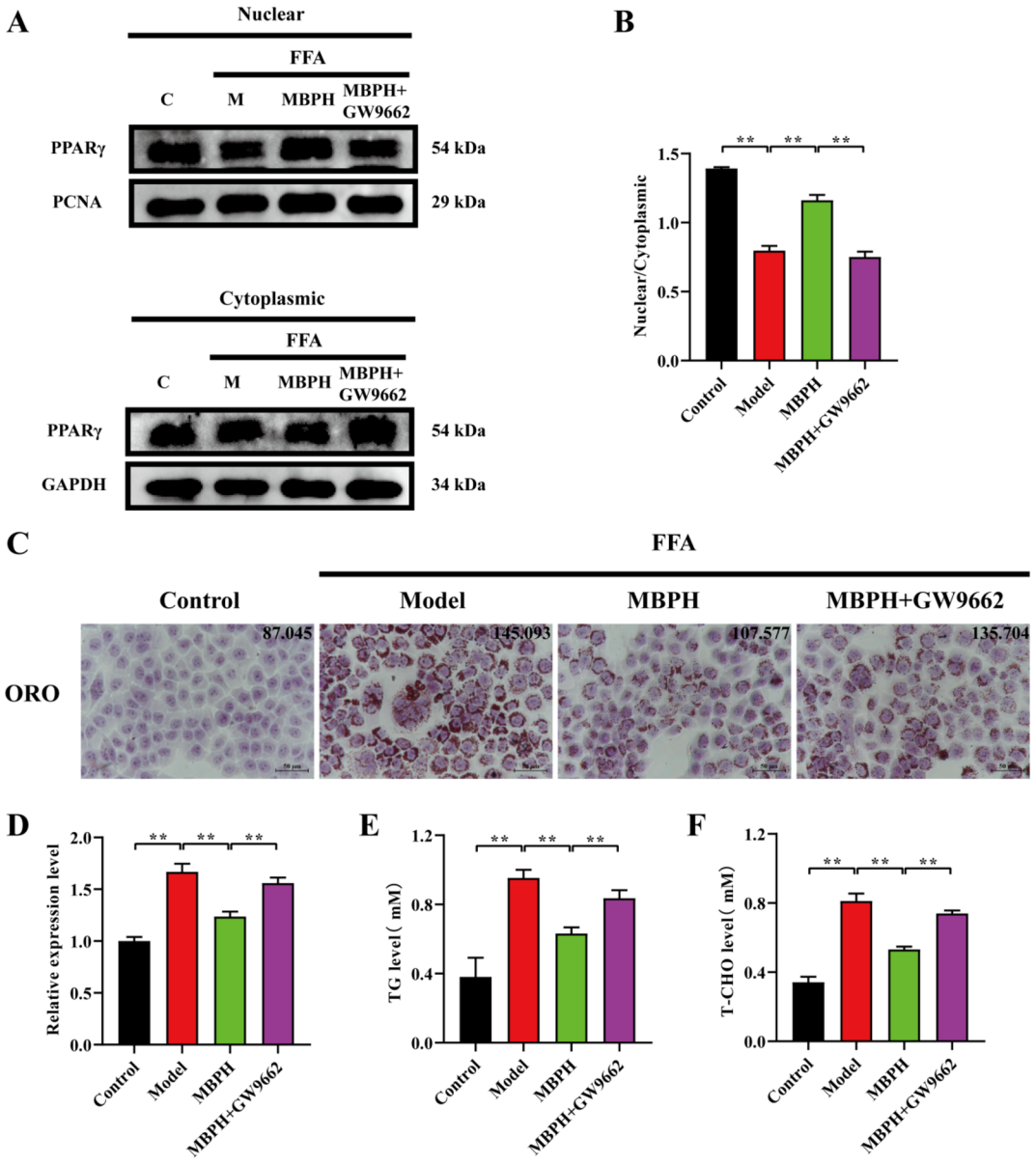


**Figure 5.** PPARγ activation is critical for the anti-NAFLD effect of MBPH. (A) Western blot analysis of PPARγ in HepG2 cells induced by FFAs. PCNA and GAPDH served as a loading control. (B) Ratio of PPARγ in nuclear to cytoplasmic protein using ImageJ software. Values are expressed as the mean ± SD ($n \geq 3$/group). (*) $p < 0.05$ and (**) $p < 0.01$ compared to the model group and the MBPH + GW9662 group. (C) Lipid phagocytosis with MBPH and GW9662 co-treatment was measured by oil red O staining in HepG2 cells. Scale bar = 50 μm. (D) Dyeing area in HepG2 cells was analyzed using ImageJ software. Values are expressed as the mean ± SD ($n \geq 3$/group). (*) $p < 0.05$ and (**) $p < 0.01$ compared to the model group and the MBPH + GW9662 group. (E) TG levels in the HepG2 cell. Values are expressed as the mean ± SD ($n \geq 3$/group). (*) $p < 0.05$ and (**) $p < 0.01$ compared to the model group and the MBPH + GW9662 group. (F) T-CHO levels in the HepG2 cell. Values are expressed as the mean ± SD ($n \geq 3$/group). (*) $p < 0.05$ and (**) $p < 0.01$ compared to the model group and the MBPH + GW9662 group.

observed by the western blot assay, which showed the same trend as qPCR results (panels D−F of Figure 3). These data suggest that MBPH may play the anti-NAFLD effect by inhibiting the fatty acid uptake *in vivo* and *in vitro*.

**PPARγ Mediates the Anti-NAFLD Effect Induced by MBPH.** Steatosis, as the hallmark feature of NAFLD, occurs when the rate of hepatic fatty acid uptake from plasma or *de novo* fatty acid synthesis is greater than the rate of fatty acid oxidation and export. To further systematically investigate the molecular mechanism of MBPH against NAFLD, RNA-seq analysis was performed in mice liver tissue. Using the β-analysis employing PCA unsupervised multivariate statistical assessments, the samples of each group were distinctly clustered, while the model group was isolated from that of the remaining two groups, which indicates that the significant differential genes were screened between the model group and the other two groups in mice (Figure 4A). The volcano diagram and Venn diagram showed 314 operational taxonomic unit (OTU) similarity among the three treatment groups (panels B and C of Figure 4). Among them, six genes were closely related to the PPARγ signaling pathway, including Acsl3, Acadl, Pparg, Slc27a1, Plin5, and Acadm (Figure 4D). Meanwhile, gene set enrichment analysis (GSEA) results showed that the PPARγ signaling pathway was outstandingly enriched (Figure 4E), and interestingly, MBPH markedly affected the downstream signaling pathway of PPARγ, such as fatty acid biosynthesis, fatty acid


https://doi.org/10.1021/acs.jafc.2c08169
J. Agric. Food Chem. 2023, 71, 1628−1642

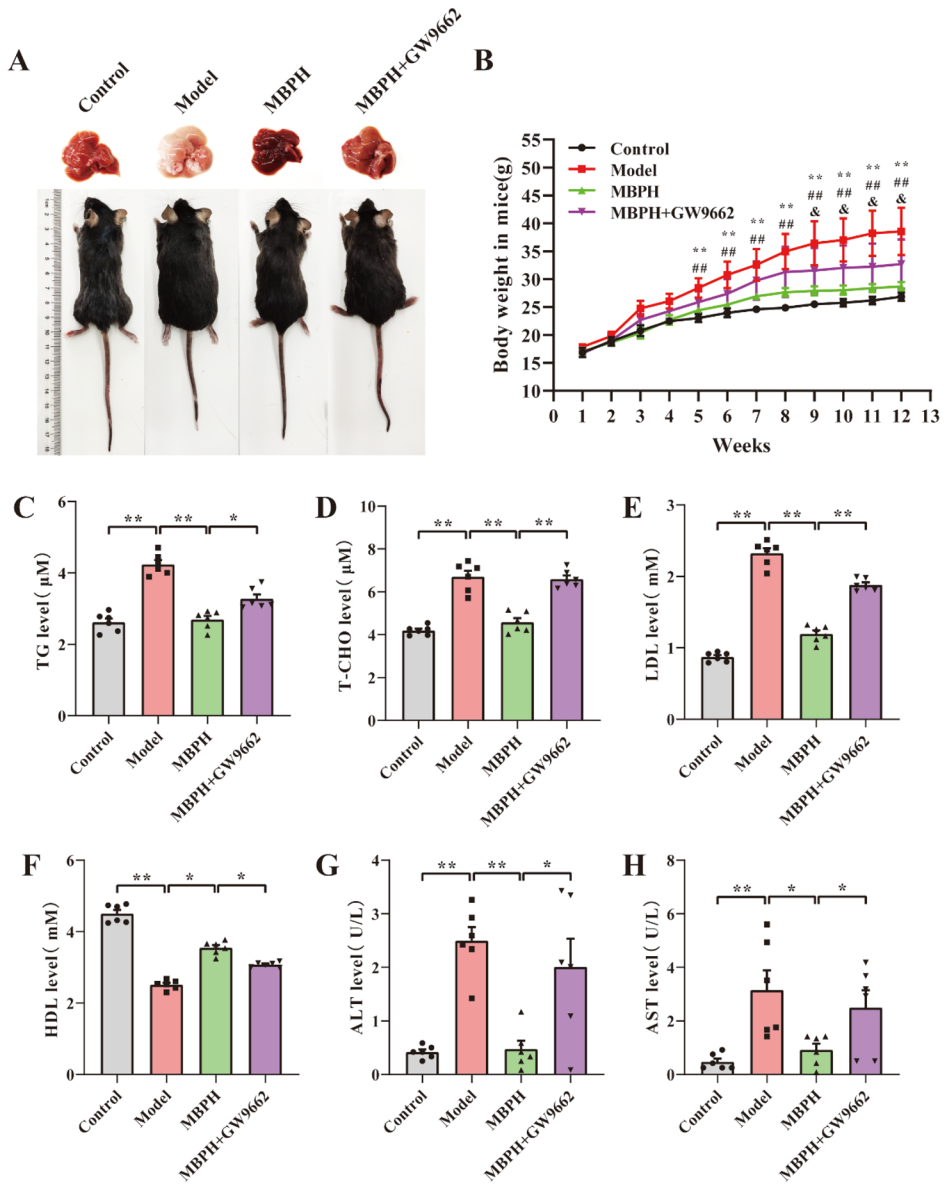


**Figure 6.** PPARγ inhibitor eliminates the anti-NAFLD effect of MBPH. (A) Representative photos of the mice and livers. (B) Effect of MBPH in mice fed the HFD on body weight. The weight change of four groups (mean ± SD). The black line marks the control group; the red line marks the model group; the green line marks the MBPH group; and the purple line marks the MBPH + GW9662 group. Values are expressed as the mean ± SD ($n \geq 6$/group). (*) $p < 0.05$ and (**) $p < 0.01$ of the control versus model group. (#) $p < 0.05$ and (##) $p < 0.01$ of the model group versus MBPH group. (&) $p < 0.05$ and (&&) $p < 0.05$ of the MBPH group versus MBPH + GW9662 group. (C) TG levels in the liver. Values are expressed as the mean ± SD ($n \geq 6$/group). (*) $p < 0.05$ and (**) $p < 0.01$ compared to the model group and the MBPH + GW9662 group. (D) T-CHO levels in the liver. Values are expressed as the mean ± SD ($n \geq 6$/group). (*) $p < 0.05$ and (**) $p < 0.01$ compared to the model group and the MBPH + GW9662 group. (E) LDL levels in the liver. Values are expressed as the mean ± SD ($n \geq 6$/group). (*) $p < 0.05$ and (**) $p < 0.01$ compared to the model group and the MBPH + GW9662 group. (F) HDL levels in the liver. Values are expressed as the mean ± SD ($n \geq 6$/group). (*) $p < 0.05$ and (**) $p < 0.01$ compared to the model group and the MBPH + GW9662 group. (G) ALT levels in the liver. Values are expressed as the mean ± SD ($n \geq 6$/group). (*) $p < 0.05$ and (**) $p < 0.01$ compared to the model group and the MBPH + GW9662 group. (H) AST levels in the liver. Values are expressed as the mean ± SD ($n \geq 6$/group). (*) $p < 0.05$ and (**) $p < 0.01$ compared to the model group and the MBPH + GW9662 group.

elongation, fatty acid degradation, and fatty acid metabolism (Figure 4F). Hence, we infer that the PPARγ signaling pathway may play an important role in the anti-NAFLD effect induced by MBPH.

**PPARγ Inhibitor Abolishes the Anti-NAFLD Effect of MBPH *in Vitro* and *in Vivo*.** To verify whether activation of the PPARγ signaling pathway is required for the anti-NAFLD effect of MBPH, a PPARγ inhibitor, GW9662, was used. The western blot assay showed that GW9662 and MBPH co-treatment markedly reversed the PPARγ activation stimulated by MBPH (panels A and B of Figure 5). The oil red O staining assay showed that the lipid accumulation in FFA-induced HepG2 cells was significantly decreased with MBPH treatment, which was blunted by GW9662 and MBPH co-treatment (panels C and D of Figure 5). Similarly, the decreased intracellular TG and T-CHO levels caused by MBPH were significantly abolished after the GW9662 and MBPH co-treatment (panels E and F of Figure 5).

To further determine the key role of the PPARγ signaling pathway in the anti-NAFLD effect of MBPH, GW9662 and


https://doi.org/10.1021/acs.jafc.2c08169
J. Agric. Food Chem. 2023, 71, 1628−1642

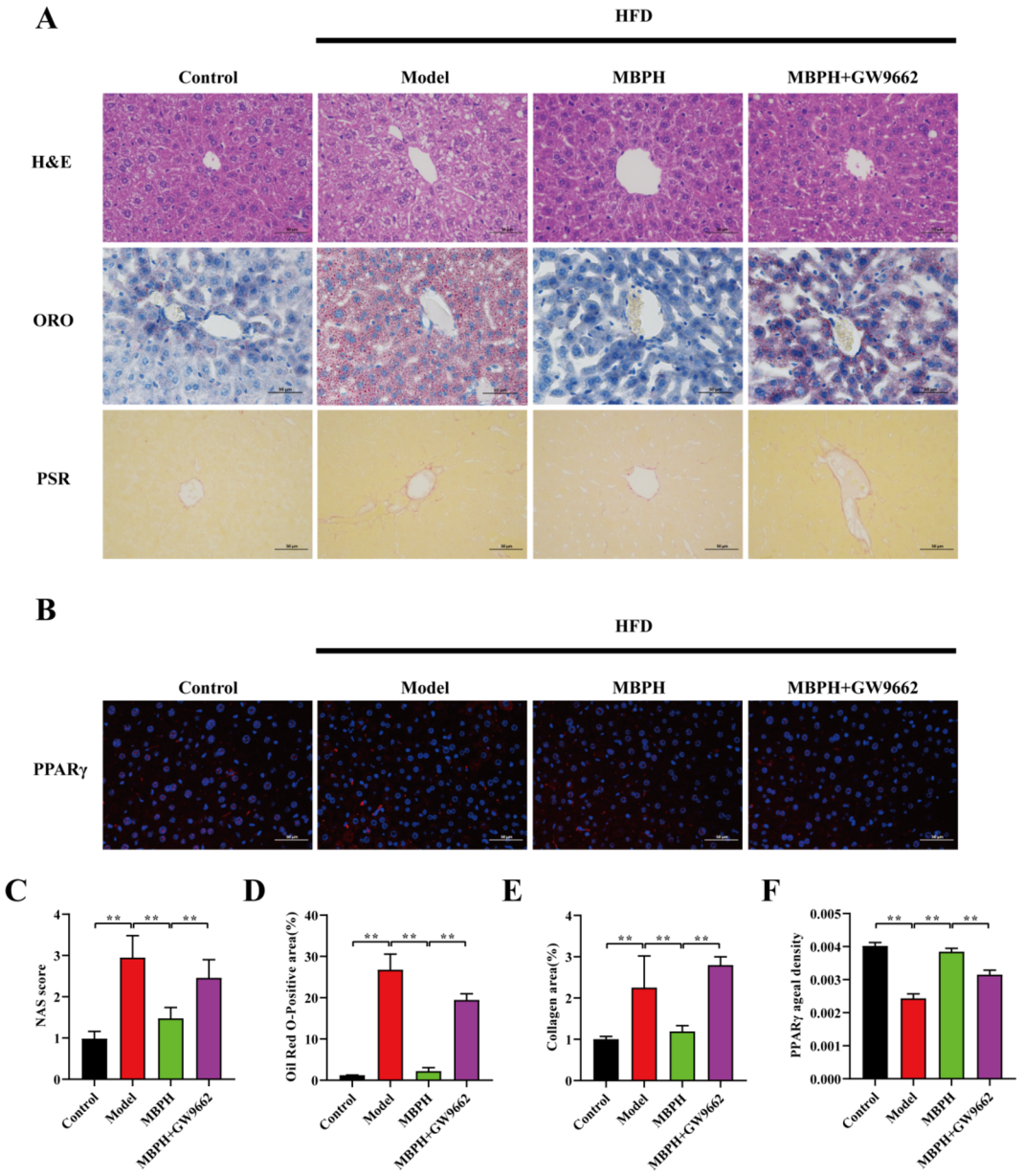


**Figure 7.** PPARγ inhibitor abolishes the attenuating effect of MBPH on hepatic steatosis. (A) Hepatic steatosis and lipid accumulation were measured by H&E, oil red O staining, and PSR staining. Scale bar = 50 μm. (B) Immunofluorescence staining of PPARγ (red) in the livers of the indicated mice fed the HFD for 12 weeks. Nuclei were labeled with DAPI (blue). Scale bar = 50 μm. (C) Hepatic steatosis was detected by the NAFLD activity score in the indicated groups. Values are expressed as the mean ± SD ($n \geq 6$/group). (*) $p < 0.05$ and (**) $p < 0.01$ compared to the model group and the MBPH + GW9662 group. (D) Dyeing area in livers was analyzed using ImageJ software. Values are expressed as the mean ± SD ($n \geq 6$/group). (*) $p < 0.05$ and (**) $p < 0.01$ compared to the model group and the MBPH + GW9662 group. (E) Collagen area in livers was analyzed using ImageJ software. Values are expressed as the mean ± SD ($n \geq 6$/group). (*) $p < 0.05$ and (**) $p < 0.01$ compared to the model group and the MBPH + GW9662 group. (F) Quantitative analyses of the relative expression of PPARγ in the livers. Values are expressed as the mean ± SD ($n \geq 6$/group). (*) $p < 0.05$ and (**) $p < 0.01$ compared to the model group and the MBPH + GW9662 group.

MBPH co-treatment was used to observe the remission effect of NAFLD in mice. Data from gross anatomy revealed that MBPH treatment markedly alleviated the hepatic steatosis in NAFLD model mice, characterized by the alleviation of hepatic vacuolar degeneration, hepatic steatosis, and fibrosis induced by HFD, which was abrogated with GW9662 and MBPH co-treatment (Figure 6A and panels A and C−E of Figure 7). In the beginning, the four groups had no obvious difference in body weight. After 5 weeks, in comparison to the control group, the body weight was significantly increased in the model group ($p < 0.01$) but had no significant difference in the MBPH group ($p > 0.05$). Noteworthy, after 9 weeks, in comparison to the MBPH group, GW9662 and MBPH co-treatment significantly increased the body weight of mice ($p < 0.01$; Figure 6B). ELISA showed that the decreased levels of TG, T-CHO, LDL, ALT, and AST of mice serum induced by MBPH as well as the enhanced HDL level were significantly recovered by GW9662 and MBPH co-treatment (panels C−H of Figure 6). Immunofluorescence staining showed that MBPH treatment significantly increased the nucleus PPARγ level in the model group, but the GW9662 and MBPH co-treatment decreased this trend (panels B and F of


https://doi.org/10.1021/acs.jafc.2c08169
J. Agric. Food Chem. 2023, 71, 1628−1642

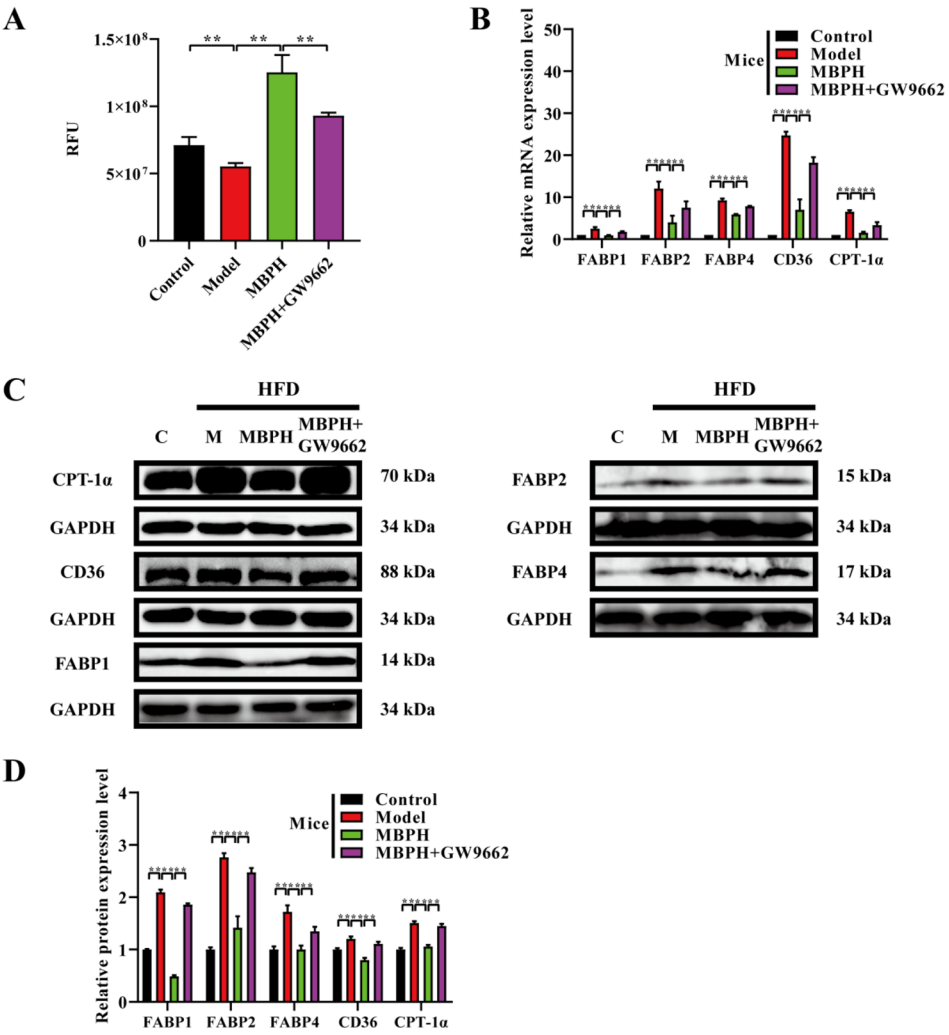


**Figure 8.** PPARγ inhibitor reverses the inhibitory effect of MBPH on fatty acid uptake in mice. (A) Fatty acid uptake in the HepG2 cell culture medium in the indicated groups was stimulated with FFAs (1.0 mM) for 24 h. Values are expressed as the mean ± SD ($n \geq 3$/group). (*) $p < 0.05$ and (**) $p < 0.01$ compared to the model group and the MBPH + GW9662 group. (B) Quantitative real-time PCR analysis of the transcript levels of genes related to fatty acid uptake (FABP1, FABP2, FABP4, CD36, and CPT-1α) *in vivo*. Gene expression was normalized to GAPDH mRNA levels. Values are expressed as the mean ± SD ($n \geq 6$/group). (*) $p < 0.05$ and (**) $p < 0.01$ compared to the model group and the MBPH + GW9662 group. (C) Expression levels of fatty-acid-uptake-related genes (FABP1, FABP2, FABP4, CD36, and CPT-1α) were measured in liver tissue of mice by western blot assays. GAPDH served as a loading control. (D) Quantitative analyses of the relative protein expression using ImageJ software *in vivo*. Values are expressed as the mean ± SD ($n \geq 6$/group). (*) $p < 0.05$ and (**) $p < 0.01$ compared to the model group and the MBPH + GW9662 group.

Figure 7). These results demonstrated that the anti-NAFLD effect of MBPH is mainly attributed to the PPARγ activation.

**PPARγ Inhibitor Effectively Reverses the Inhibitory Effect of MBPH on Fatty Acid Uptake in Mice.** To further determine PPARγ activation on fatty acid uptake *in vivo*, the fatty acid uptake related indexes were measured with GW9662 and MBPH co-treatment. The results *in vitro* showed that MBPH treatment significantly increased the content of the FFAs in the culture medium compared to the model group, but GW9962 and MBPH co-treatment partly eliminated this effect (Figure 8A). As expected, real-time PCR and western blot results also showed that MBPH treatment significantly reduced the expression levels of fatty-acid-uptake-related genes, such as FABP1, FABP2, FABP4, CD36, and CPT-1α *in vivo* and *in vitro*, and this decreased trend was significantly reversed by GW9962 and MBPH co-treatment (panels B−D of Figure 8). Collectively, these data indicate that MBPH exerts the anti-NAFLD effect mainly via activating the PPARγ signal pathway to restrain fatty acid uptake of live tissue in mice.

**MBPH Contains Peptide Components That Bind to PPARγ Activity.** Next, we analyzed the peptide fractions of activating PPARγ in MBPH by LC−MS/MS [peptide-to-spectrum match (PSM) false discovery rate (FDR) of ≤0.01], and screening criteria identified for peptides were adopted after mass spectrometry data retrieval. The results showed a total of 490 peptides were identified from MBPH, and the length of these peptides varied from 6 to 20 amino acids. These peptides were scored for activity using PeptideRanker and subjected with scores greater than 0.8 to molecular docking with PPARγ. PeptideRanker was trained at a threshold of 0.8; i.e., any peptide predicted over a 0.8 threshold is labeled as bioactive. By screening, 41 peptides whose scores are greater than 0.8 were docked with PPARγ separately, and the PPARγ binds most strongly to GQPWPPASFACR in peptides greater than 10 amino acids and most strongly to SIPAFCR in peptides less than 10 amino acids. As shown in Table 1, the predicted binding affinities of GQPWPPASFACR and SIPAFCR were −9.0 and −8.5 kcal/mol, respectively, indicating that GQPWPPASFACR


https://doi.org/10.1021/acs.jafc.2c08169
J. Agric. Food Chem. 2023, 71, 1628−1642

**Table 1. Identification of Peptide Components in MBPH with PPARγ Binding Activity**

| sequence | length | mass | leading razor protein | start position | end position | score | PeptideRanker score | Vina score (PPARγ) (kcal/mol) |
|---|---|---|---|---|---|---|---|---|
| GQGSAPSAGCCNGVR | 15 | 1476.62 | K3ZKC1 | 44 | 58 | 185.08 | 0.858302 | −7.8 |
| AWPCCDTCGVCTR | 13 | 1641.616 | K4AGV5 | 43 | 55 | 172.88 | 0.937971 | −6.8 |
| IPPSDSCCR | 9 | 1090.454 | K3XNF9 | 49 | 57 | 170.73 | 0.829101 | −6.6 |
| SQPPICHCWDEVKR | 14 | 1810.824 | K3XLQ3 | 159 | 172 | 166.86 | 0.855924 | −6.4 |
| QGLISDPVFSFWFNR | 15 | 1811.9 | K3Z5J2 | 212 | 226 | 160.53 | 0.910062 | −7.2 |
| GQPWPPASFACR | 12 | 1372.635 | A0A368SRA4 | 78 | 89 | 140.45 | 0.970927 | −9.0 |
| SIPPLCQCLDAVPR | 14 | 1624.807 | K4AJ19 | 67 | 80 | 138.25 | 0.837931 | −6.2 |
| CRDFLPEGCPCK | 12 | 1537.648 | A0A368R2U0 | 123 | 134 | 136.96 | 0.858289 | −6.7 |
| VACHWECFNK | 10 | 1349.565 | K3XN79 | 52 | 61 | 134.81 | 0.836014 | −7.1 |
| QGPNLNGLFGR | 11 | 1171.61 | K3ZB68 | 37 | 47 | 129.47 | 0.893153 | −7.5 |
| GVPVWHCCCPR | 11 | 1426.606 | K3ZKJ5 | 80 | 90 | 123.69 | 0.957586 | −6.7 |
| SLPPICSCR | 9 | 1088.511 | K4AGV5 | 56 | 64 | 122.74 | 0.876192 | −6.4 |
| GDLQWCR | 7 | 933.4127 | K3ZIP9 | 51 | 57 | 119.57 | 0.86484 | −7.9 |
| SWPPICR | 7 | 914.4433 | K3XLQ3 | 78 | 84 | 118.06 | 0.959344 | −7.1 |
| ACCFACITAGGSDSLCK | 17 | 1876.758 | K3ZKL3 | 40 | 56 | 117.23 | 0.925819 | −6.2 |
| CCSLPICTR | 9 | 1165.504 | K3XLQ3 | 150 | 158 | 115.49 | 0.874376 | −6.2 |
| CCDLAMCMR | 9 | 1215.433 | K3XLQ3 | 69 | 77 | 115.46 | 0.95532 | −6.8 |
| GPFVPLPAIR | 10 | 1065.634 | K4A046 | 60 | 69 | 114.78 | 0.892796 | −7.8 |
| SCIPQEVGWLR | 11 | 1343.666 | K3ZUA5 | 253 | 263 | 104.17 | 0.82291 | −7.7 |
| SIPAFCR | 7 | 849.4167 | A0A368R2P3 | 71 | 77 | 98.03 | 0.907681 | −8.5 |
| QPGGWTAGYCR | 11 | 1251.546 | K3YLU9 | 61 | 71 | 97.431 | 0.862308 | −8.3 |
| RANCSCGPNCNCASCSATA | 19 | 2116.76 | A0A368SQH9 | 66 | 84 | 96.756 | 0.8439 | −6.4 |
| RPWKCCSLPICTR | 13 | 1732.832 | K3XLQ3 | 146 | 158 | 92.112 | 0.921918 | −6.0 |
| LVPGWTKPICIGR | 13 | 1495.833 | K3XIC0 | 122 | 134 | 85.29 | 0.815492 | −7.2 |
| QQCSPTPTPYCSPQCQMLR | 19 | 2337.996 | A0A368Q182 | 51 | 69 | 81.239 | 0.835062 | −6.9 |
| SLLIPFR | 7 | 844.5171 | K4AD89 | 27 | 33 | 80.377 | 0.843411 | −7.3 |
| GAPLFQCTDFITNFCK | 16 | 1917.875 | K4AGV5 | 88 | 103 | 78.136 | 0.868052 | −7.2 |
| ACCFGCIAVGGTDAVCK | 17 | 1844.768 | K3ZKR6 | 40 | 56 | 72.958 | 0.880762 | −6.0 |
| GLSFDFYK | 8 | 975.4702 | K3XJE1 | 40 | 47 | 72.875 | 0.824943 | −8.1 |
| SFAADVDLEDLGLNCFWK | 18 | 2098.967 | K4A4W1 | 176 | 193 | 72.652 | 0.851087 | −5.3 |
| SQPPICHCWDEVK | 13 | 1654.723 | K3XLQ3 | 159 | 171 | 72.652 | 0.811088 | −6.8 |
| CGCAVPCPGGK | 11 | 1161.473 | A0A368SQH9 | 7 | 17 | 72.485 | 0.957049 | −6.9 |
| PDPEPCFR | 8 | 1016.439 | K3ZKJ5 | 38 | 45 | 69.176 | 0.922958 | −8.2 |
| GSDCVDPFIALQNCIR | 16 | 1863.861 | K3YWH2 | 84 | 99 | 67.022 | 0.872282 | −5.1 |
| GQGSKPSDACCSGVK | 15 | 1536.666 | K3YAY4 | 44 | 58 | 66.56 | 0.824695 | −5.7 |
| IPPSDGCCGLVK | 12 | 1301.611 | Q7XBG4 | 49 | 60 | 63.076 | 0.834198 | −6.6 |
| SGPFFFISGNEASCR | 15 | 1674.746 | K3XYR7 | 100 | 114 | 61.235 | 0.847996 | −6.8 |
| NVCLVWGCCPIK | 12 | 1504.699 | K3Z621 | 401 | 412 | 58.916 | 0.85803 | −6.2 |
| AGDVFWIPRFFAFCQVAAR | 19 | 2257.126 | A0A368SRA4 | 399 | 417 | 40.179 | 0.926271 | −7.1 |
| GDWDRLFRHCNPSYLR | 16 | 2090.986 | K3ZTC3 | 255 | 270 | 39.918 | 0.872362 | −5.6 |
| FCGVLPDTFLHLR | 13 | 1573.808 | A0A368QYR5 | 76 | 88 | 39.016 | 0.894415 | −6.2 |

and SIPAFCR can bind stably to PPARγ and have the potential to activate PPARγ. Validation of GQPWPPASFACR and SIPAFCR for the anti-NAFLD effect is worth our further in-depth study.

## DISCUSSION

In recent years, there is growing interest in plant peptide products for the prevention and treatment of NAFLD. For example, the study by Lemus-Conejo et al. showed that a lupine (*Lupinus angustifolious* L.) peptide alleviates HFD-induced NAFLD in mice.[21] Zhao et al. found that rapeseed peptide could ameliorate non-alcoholic steatohepatitis and related metabolic disorders in mice.[22] Kawaguchi et al. showed that peptides derived from wheat bran alleviate NAFLD in the HFD-fed mice model by inhibiting oxidative stress and upregulating the AMPK/ACC pathway.[23] Therefore, these studies indicate that plant peptides as the drugs for anti-NAFLD have a great development prospect. In the present study, we found that MBPH obtained by *in vitro* simulated bionic digestion exhibited significant anti-NAFLD activity in HFD-induced mice and the FFA-induced HepG2 cell, characterized by hepatic steatosis and lipid accumulation (Figures 1 and 2), indicating that MBPH has the potential to develop as a natural supplement for the prevention of NAFLD.

NAFLD arises when the fatty acid uptake is greater than the rate of fatty acid β-oxidation, which is indicative of the importance of fatty acid uptake in NAFLD pathogenesis. Hence, restraining the rate of fatty acid uptake in the liver may become a new treatment strategy of intervening NAFLD.[3,24] Fatty acid binding proteins (FABPs) are a lipid-binding protein family of lipid transporters with affinity for long-chain fatty acids and other ligands. FABP1 highly expressed in liver tissue facilitates the uptake and metabolism of long-chain fatty acids *in vitro* and in cultured cells, and the abnormal expression or loss of FABP1 will reduce hepatic long-chain fatty acid uptake.[25] The


https://doi.org/10.1021/acs.jafc.2c08169
J. Agric. Food Chem. 2023, 71, 1628−1642

studies showed that FABP2 and FABP4 can be abnormally upregulated in other diseased tissues and organs, such as the liver in NAFLD.[26,27] CD36, a fatty acid translocase, mediates the uptake of FFAs from circulation and intracellular transport of long-chain fatty acids in a variety of cell types, such as macrophages, microvascular endothelial cells, adipocytes, muscle cells, enterocytes, and hepatocytes,[28,29] and was especially highly expressed in the liver tissue of HFD-induced fatty liver mice and those of human NAFLD.[29] Therefore, the abnormal expression of FABP1, FABP2, FABP4, and CD36 in liver tissue may promote the occurrence and development of NAFLD. Our present result showed that MBPH significantly downregulated the expression levels of fatty-acid-uptake-related genes (FABP1, FABP2, FABP4, and CD36) *in vivo* and *in vitro*, which contributes to the decrease of the ratio of fatty acid uptake (Figure 3). Therefore, MBPH can act as a negative regulator of fatty acid uptake, thereby affecting NAFLD formation and development *in vivo* and *in vitro*. In addition, CPT-1$\alpha$, as a rate-limiting enzyme of FFA $\beta$-oxidation, is essential for regulating the rate of the $\beta$-oxidation pathway in the liver.[30] Although the inhibition of CPT-1$\alpha$ led to a decrease in the fatty acid oxidation (FAO) rate, MBPH markedly inhibited the fatty acid uptake in the NAFLD model (Figures 3 and 8), and hence, we speculate that the reduction in lipid storage is mainly attributed to the significant decrease of fatty acid uptake. In addition, Sun et al. showed that liver with deficient CPT-1$\alpha$ expression can protect against HFD-evoked liver damage and potentiates adipose browning in a FGF21-dependent manner, which may serve as a viable strategy for the treatment of obesity and NAFLD.[31] Therefore, MBPH downregulates CPT-1$\alpha$ expression, which also contributes to its anti-NAFLD effect.

Peroxisome proliferator-activated receptors (PPARs), which are nuclear receptor proteins, are involved in a wide variety of regulatory functions,[32] and the conformation changes of PPAR$\gamma$ induced by binding ligand recruit some of the transcriptional coactivators and, thus, initiate the transcription of downstream genes to regulate the glucose and lipid metabolism and immune response and promote cell differentiation.[33,34] Dysregulation of PPAR$\gamma$ is linked to the development of obesity, type 2 diabetes (T2D), atherosclerosis, and other disease conditions.[35,36] Oppositely, PPAR$\gamma$ activation supports the formation of healthy adipose tissue, thereby preventing shunting of excess lipids to the liver and the formation of dysfunctional adipocytes.[37] In hepatocytes, PPAR$\gamma$ is a regulator of lipid metabolism,[38] and its upregulation can inhibit the expression levels of the downstream fatty-acid-uptake-related genes (FABP1, FABP4, and CPT-1$\alpha$).[39−41] Jahandideh et al. showed that active peptides isolated from natural products were able to act as activators of PPAR$\gamma$.[42] Liu et al. found that some peptides can activate the transcription of PPAR$\gamma$ and regulate downstream gene expression, thus suppressing adipogenesis and obesity.[43] Interestingly, our study showed that PPAR$\gamma$ was significantly activated by MBPH treatment by transcriptome in liver tissue of mice (Figure 4) and the HepG2 cell induced by FFAs and the PPAR$\gamma$ activation was negatively correlated with the lipid accumulation (Figure 5). Similarly, the validation results *in vivo* and *in vitro* showed that the anti-NAFLD effect of MBPH could be abolished by the PPAR$\gamma$ inhibitor (GW9662; Figures 6−8), which indicates that PPAR$\gamma$ activation plays a crucial role in MBPH-induced anti-NAFLD.

PPAR$\gamma$ full agonists are used in clinical treatment as antidiabetic agents to treat T2D by increasing insulin sensitivity, improving glycemic control, and lowering blood glucose, such as the most representative thiazolidine-2,4-dione (TZD) group.[44] However, recent studies showed that PPAR$\gamma$ full agonists have some side effects, such as significant weight gain, peripheral edema, increased risk of congestive heart failure, and higher bone fracture rate, which have restrained their clinical use.[45] In contrast, selective PPAR$\gamma$ modulators (SPPAR$\gamma$Ms), as novel PPAR$\gamma$ ligands, can selectively activate PPAR$\gamma$ in different ways to distinct downstream genes, which may have potential in managing obesity, T2D, dyslipidemia, and NAFLD.[44] On the basis of our results thus far, MBPH acts as an anti-NAFLD activity by activating PPAR$\gamma$ and has no side effect in mice (Figures 2 and 8), which indicates that MBPH may contain the active peptide components of selective PPAR$\gamma$ modulators. Next, we analyzed the peptide fractions of activating PPAR$\gamma$ in MBPH by LC−MS/MS and subjected them with scores greater than 0.8 by PeptideRanker to molecular docking with PPAR$\gamma$. Two peptides (GQPWPPASFACR and SIPAFCR) with strong PPAR$\gamma$ binding ability were identified (Table 1), and they were supplied as the potential selective activator of PPAR$\gamma$ and are worth a further in-depth study.

In conclusion, MBPH obtained by *in vitro* simulated bionic digestion displays outstanding anti-NAFLD activity *in vivo* and *in vitro*. Further, we found that MBPH treatment significantly attenuated hepatic steatosis and lipid accumulation through activating PPAR$\gamma$ to restrain the fatty acid uptake, which exerts the anti-NAFLD effect. The highlights of the current study lies in elucidating that MBPH have the potential to be developed as a new generation of nutritional supplements for the prevention and treatment of NAFLD.

## ■ ASSOCIATED CONTENT

### Supporting Information

The Supporting Information is available free of charge at https://pubs.acs.org/doi/10.1021/acs.jafc.2c08169.

Sequence information on gene primers (Table S1) and interaction between MBPH and PPAR$\gamma$ (Figure S1) (PDF)

## ■ AUTHOR INFORMATION


### Corresponding Authors

**Zhuoyu Li** − *Key Laboratory of Chemical Biology and Molecular Engineering of National Ministry of Education, Institute of Biotechnology, Shanxi University, Taiyuan, Shanxi 030006, People's Republic of China*; orcid.org/0000-0003-3979-0487; Phone: +86-351-7018268; Email: lzy@sxu.edu.cn

**Shuhua Shan** − *Key Laboratory of Chemical Biology and Molecular Engineering of National Ministry of Education, Institute of Biotechnology, Shanxi University, Taiyuan, Shanxi 030006, People's Republic of China*; Phone: +86-351-7011499; Email: ssh@sxu.edu.cn

### Authors

**Jiaqi Zhou** − *Key Laboratory of Chemical Biology and Molecular Engineering of National Ministry of Education, Institute of Biotechnology, Shanxi University, Taiyuan, Shanxi 030006, People's Republic of China*

**Ruopeng Yin** − *State Key Laboratory of Mycology, Institute of Microbiology, Chinese Academy of Sciences, Beijing 100101, People's Republic of China*

**Lizhen Zhang** − *School of Life Science, Shanxi University, Taiyuan, Shanxi 030006, People's Republic of China*

**Jiangying Shi** − *Key Laboratory of Chemical Biology and Molecular Engineering of National Ministry of Education, Institute of Biotechnology, Shanxi University, Taiyuan, Shanxi 030006, People's Republic of China*

**Qinqin Qiao** − *Key Laboratory of Chemical Biology and Molecular Engineering of National Ministry of Education, Institute of Biotechnology, Shanxi University, Taiyuan, Shanxi 030006, People's Republic of China*

Complete contact information is available at: https://pubs.acs.org/10.1021/acs.jafc.2c08169

### Author Contributions

†Shuhua Shan and Jiaqi Zhou contributed equally to this work.

### Funding

This study was supported by the National Natural Science Foundation of China (32270420 and 32072220), the National Key Research and Development Project (2020YFD1001405), the Shanxi Province Science Foundation (202103021224011), and the Shanxi Key Laboratory for Research and Development of Regional Plants.

### Notes

The authors declare no competing financial interest.

## REFERENCES

(1) Ipsen, D. H.; Lykkesfeldt, J.; Tveden-Nyborg, P. Molecular mechanisms of hepatic lipid accumulation in non-alcoholic fatty liver disease. *Cell. Mol. Life Sci.* **2018**, *75* (18), 3313−3327.

(2) Milić, S.; Lulić, D.; Štimac, D. Non-alcoholic fatty liver disease and obesity: Biochemical, metabolic and clinical presentations. *World J. Gastroenterol.* **2014**, *20* (28), 9330−9337.

(3) Mato, J. M.; Alonso, C.; Noureddin, M.; Lu, S. C. Biomarkers and subtypes of deranged lipid metabolism in non-alcoholic fatty liver disease. *World J. Gastroenterol.* **2019**, *25* (24), 3009−3020.

(4) Shi, T.; Yu, L.; Zhuang, R.; Xi, J.; He, R.; Shao, Y.; Huang, J.; Liu, S.; Yang, X. Regulation of Mitochondrial Function by Natural Products for the Treatment of Metabolic Associated Fatty Liver Disease. *Can. J. Gastroenterol. Hepatol.* **2021**, *2021*, 1−9.

(5) Yu, Y.; Gaine, G. K.; Zhou, L.; Zhang, J.; Wang, J.; Sun, B. The classical and potential novel healthy functions of rice bran protein and its hydrolysates. *Crit. Rev. Food Sci. Nutr.* **2022**, *62* (30), 8454−8466.

(6) Zanoni, C.; Aiello, G.; Arnoldi, A.; Lammi, C. Investigations on the hypocholesterolaemic activity of LILPKHSDAD and LTFPGSAED, two peptides from lupin $\beta$-conglutin: Focus on LDLR and PCSK9 pathways. *J. Funct. Foods* **2017**, *32*, 1−8.

(7) Ashraf, J.; Awais, M.; Liu, L.; Khan, M. I.; Tong, L.-T.; Ma, Y.; Wang, L.; Zhou, X.; Zhou, S. Effect of thermal processing on cholesterol synthesis, solubilisation into micelles and antioxidant activities using peptides of *Vigna angularis* and *Vicia faba*. *LWT* **2020**, *129*, 109504.

(8) Alashi, A. M.; Blanchard, C. L.; Mailer, R. J.; Agboola, S. O.; Mawson, A. J.; Aluko, R. E.; Strappe, P. Effects of canola proteins and hydrolysates on adipogenic differentiation of C3H10T/2 mesenchymal stem cells. *Food Chem.* **2015**, *185*, 226−32.

(9) Georgoulis, M.; Kontogianni, M. D.; Tileli, N.; Margariti, A.; Fragopoulou, E.; Tiniakos, D.; Zafiropoulou, R.; Papatheodoridis, G. The impact of cereal grain consumption on the development and severity of non-alcoholic fatty liver disease. *Eur. J. Nutr.* **2014**, *53* (8), 1727−1735.

(10) Ye, E. Q.; Chacko, S. A.; Chou, E. L.; Kugizaki, M.; Liu, S. Greater whole-grain intake is associated with lower risk of type 2 diabetes, cardiovascular disease, and weight gain. *J. Nutr.* **2012**, *142* (7), 1304−13.

(11) Murtaugh, M. A.; Jacobs, D. R., Jr.; Jacob, B.; Steffen, L. M.; Marquart, L. Epidemiological support for the protection of whole grains against diabetes. *Proc. Nutr. Soc.* **2003**, *62* (1), 143−9.

(12) Murtaza, N.; Baboota, R. K.; Jagtap, S.; Singh, D. P.; Khare, P.; Sarma, S. M.; Podili, K.; Alagesan, S.; Chandra, T. S.; Bhutani, K. K.; Boparai, R. K.; Bishnoi, M.; Kondepudi, K. K. Finger millet bran supplementation alleviates obesity-induced oxidative stress, inflammation and gut microbial derangements in high-fat diet-fed mice. *Br. J. Nutr.* **2014**, *112* (9), 1447−1458.

(13) Boonloh, K.; Kukongviriyapan, V.; Kongyingyoes, B.; Kukongviriyapan, U.; Thawornchinsombut, S.; Pannangpetch, P. Rice Bran Protein Hydrolysates Improve Insulin Resistance and Decrease Pro-inflammatory Cytokine Gene Expression in Rats Fed a High Carbohydrate-High Fat Diet. *Nutrients* **2015**, *7* (8), 6313−6329.

(14) Naik, H. S.; Srilatha, C.; Sujatha, K.; Sreedevi, B.; Prasad, T. N. V. K. V. Supplementation of whole grain flaxseeds (*Linum usitatissimum*) along with high cholesterol diet and its effect on hyperlipidemia and initiated atherosclerosis in Wistar albino male rats. *Vet. World* **2018**, *11* (10), 1433−1439.

(15) Ofosu, F. K.; Mensah, D.-J. F.; Daliri, E. B.-M.; Oh, D.-H. Exploring Molecular Insights of Cereal Peptidic Antioxidants in Metabolic Syndrome Prevention. *Antioxidants* **2021**, *10* (4), 518.

(16) Acosta-Estrada, B. A.; Gutiérrez-Uribe, J. A.; Serna-Saldívar, S. O. Bound phenolics in foods, a review. *Food Chem.* **2014**, *152*, 46−55.

(17) Shan, S.; Yin, R.; Shi, J.; Zhang, L.; Liu, F.; Qiao, Q.; Li, Z. Bowman-Birk Major Type Trypsin Inhibitor Derived from Foxtail Millet Bran Attenuate Atherosclerosis via Remodeling Gut Microbiota in ApoE−/− Mice. *J. Agric. Food Chem.* **2022**, *70* (2), 507−519.

(18) Shan, S.; Wu, C.; Shi, J.; Zhang, X.; Niu, J.; Li, H.; Li, Z. Inhibitory Effects of Peroxidase from Foxtail Millet Bran on Colitis-Associated Colorectal Carcinogenesis by the Blockage of Glycerophospholipid Metabolism. *J. Agric. Food Chem.* **2020**, *68* (31), 8295−8307.

(19) Cheng, X.; Geng, F.; Pan, M.; Wu, X.; Zhong, Y.; Wang, C.; Tian, Z.; Cheng, C.; Zhang, R.; Puduvalli, V.; Horbinski, C.; Mo, X.; Han, X.; Chakravarti, A.; Guo, D. Targeting DGAT1 Ameliorates Glioblastoma by Increasing Fat Catabolism and Oxidative Stress. *Cell Metab.* **2020**, *32* (2), 229−242.

(20) Guo, D.; Hildebrandt, I. J.; Prins, R. M.; Soto, H.; Mazzotta, M. M.; Dang, J.; Czernin, J.; Shyy, J. Y.; Watson, A. D.; Phelps, M.; Radu, C. G.; Cloughesy, T. F.; Mischel, P. S. The AMPK agonist AICAR inhibits the growth of EGFRvIII-expressing glioblastomas by inhibiting lipogenesis. *Proc. Natl. Acad. Sci. U.S.A.* **2009**, *106* (31), 12932−7.

(21) Lemus-Conejo, A.; Grao-Cruces, E.; Toscano, R.; Varela, L. M.; Claro, C.; Pedroche, J.; Millan, F.; Millan-Linares, M. C.; Montserrat-de la Paz, S. A lupine (*Lupinus angustifolious* L.) peptide prevents non-alcoholic fatty liver disease in high-fat-diet-induced obese mice. *Food Funct.* **2020**, *11* (4), 2943−2952.

(22) Zhao, Q.; Xu, H.; Hong, S.; Song, N.; Xie, J.; Yan, Z.; Wang, R.; Yang, P.; Jiang, X. Rapeseed Protein-Derived Antioxidant Peptide RAP Ameliorates Nonalcoholic Steatohepatitis and Related Metabolic Disorders in Mice. *Mol. Pharmaceutics* **2019**, *16* (1), 371−381.

(23) Kawaguchi, T.; Ueno, T.; Nogata, Y.; Hayakawa, M.; Koga, H.; Torimura, T. Wheat-bran autolytic peptides containing a branched-chain amino acid attenuate non-alcoholic steatohepatitis via the suppression of oxidative stress and the upregulation of AMPK/ACC in high-fat diet-fed mice. *Int. J. Mol. Med.* **2017**, *39* (2), 407−414.

(24) Kawano, Y.; Cohen, D. E. Mechanisms of hepatic triglyceride accumulation in non-alcoholic fatty liver disease. *J. Gastroenterol.* **2013**, *48* (4), 434−441.

(25) Atshaves, B. P.; Martin, G. G.; Hostetler, H. A.; McIntosh, A. L.; Kier, A. B.; Schroeder, F. Liver fatty acid-binding protein and obesity. *J. Nutr. Biochem.* **2010**, *21* (11), 1015−32.

(26) Pishva, H.; Amini, M.; Eshraghian, M. R.; Hosseini, S.; Mahboob, S. A. Effects of EPA supplementation on plasma fatty acids composition in hypertriglyceridemic subjects with FABP2 and PPAR$\alpha$ genotypes. *J. Diabetes Metab. Disord.* **2012**, *11* (1), 25.

(27) Thompson, K. J.; Austin, R. G.; Nazari, S. S.; Gersin, K. S.; Iannitti, D. A.; McKillop, I. H. Altered fatty acid-binding protein 4 (FABP4) expression and function in human and animal models of hepatocellular carcinoma. *Liver Int.* **2018**, *38* (6), 1074−1083.

(28) Su, X.; Abumrad, N. A. Cellular fatty acid uptake: A pathway under construction. *Trends Endocrinol. Metab.* **2009**, *20* (2), 72−77.

(29) Iio, A.; Ito, M.; Itoh, T.; Terazawa, R.; Fujita, Y.; Nozawa, Y.; Ohsawa, I.; Ohno, K.; Ito, M. Molecular hydrogen attenuates fatty acid uptake and lipid accumulation through downregulating CD36 expression in HepG2 cells. *Med. Gas Res.* **2013**, *3* (1), 6.
(30) Zhang, L.; Keung, W.; Samokhvalov, V.; Wang, W.; Lopaschuk, G. D. Role of fatty acid uptake and fatty acid $\beta$-oxidation in mediating insulin resistance in heart and skeletal muscle. *Biochim. Biophys. Acta, Mol. Cell Biol. Lipids* **2010**, *1801* (1), 1−22.
(31) Sun, W.; Nie, T.; Li, K.; Wu, W.; Long, Q.; Feng, T.; Mao, L.; Gao, Y.; Liu, Q.; Gao, X.; Ye, D.; Yan, K.; Gu, P.; Xu, Y.; Zhao, X.; Chen, K.; Loomes, K. M.; Lin, S.; Wu, D.; Hui, X. Hepatic CPT1A Facilitates Liver-Adipose Cross-Talk via Induction of FGF21 in Mice. *Diabetes* **2022**, *71* (1), 31−42.
(32) Desvergne, B.; Wahli, W. Peroxisome proliferator-activated receptors: Nuclear control of metabolism. *Endocr. Rev.* **1999**, *20* (5), 649−688.
(33) Wagner, N.; Wagner, K.-D. The Role of PPARs in Disease. *Cells* **2020**, *9* (11), 2367.
(34) Apostoli, A. J.; Nicol, C. J. B. PPAR Medicines and Human Disease: The ABCs of It All. *PPAR Res.* **2012**, *2012*, 1−16.
(35) Janani, C.; Ranjitha Kumari, B. D. PPAR gamma gene—A review. *Diabetes Metab. Syndr.* **2015**, *9* (1), 46−50.
(36) Lehrke, M.; Lazar, M. A. The Many Faces of PPAR$\gamma$. *Cell* **2005**, *123* (6), 993−999.
(37) Skat-Rørdam, J.; Højland Ipsen, D.; Lykkesfeldt, J.; Tveden-Nyborg, P. A role of peroxisome proliferator-activated receptor $\gamma$ in non-alcoholic fatty liver disease. *Basic Clin. Pharmacol. Toxicol.* **2019**, *124* (5), 528−537.
(38) AlNafea, H. M.; Korish, A. A. Activation of the Peroxisome Proliferator-Activated Receptors (PPAR-$\alpha/\gamma$) and the Fatty Acid Metabolizing Enzyme Protein CPT1A by Camel Milk Treatment Counteracts the High-Fat Diet-Induced Nonalcoholic Fatty Liver Disease. *PPAR Res.* **2021**, *2021*, 5558731.
(39) Wang, Z.; Yue, Y. X.; Liu, Z. M.; Yang, L. Y.; Li, H.; Li, Z. J.; Li, G. X.; Wang, Y. B.; Tian, Y. D.; Kang, X. T.; Liu, X. J. Genome-Wide Analysis of the FABP Gene Family in Liver of Chicken (*Gallus gallus*): Identification, Dynamic Expression Profile, and RegulatoryMechanism. *Int. J. Mol. Sci.* **2019**, *20* (23), 5948.
(40) Tu, J.; Zhu, S.; Li, B.; Xu, G.; Luo, X.; Jiang, L.; Yan, X.; Zhang, R.; Chen, C. Gegen Qinlian Decoction Coordinately Regulates PPAR$\gamma$ and PPAR$\alpha$ to Improve Glucose and Lipid Homeostasis in Diabetic Rats and Insulin Resistance 3T3-L1 Adipocytes. *Front. Pharmacol.* **2020**, *11*, 811.
(41) Xu, L.; Xia, H.; Ni, D.; Hu, Y.; Liu, J.; Qin, Y.; Zhou, Q.; Yi, Q.; Xie, Y. High-Dose Dexamethasone Manipulates the Tumor Microenvironment and Internal Metabolic Pathways in Anti-Tumor Progression. *Int. J. Mol. Sci.* **2020**, *21* (5), 1846.
(42) Jahandideh, F.; Liu, P.; Wu, J. Purification and identification of adipogenic-differentiating peptides from egg white hydrolysate. *Food Chem.* **2018**, *259*, 25−30.
(43) Liu, Y.; Luo, B.; Shi, R.; Wang, J.; Liu, Z.; Liu, W.; Wang, S.; Zhang, Z. Nonerythropoietic Erythropoietin-Derived Peptide Suppresses Adipogenesis, Inflammation, Obesity and Insulin Resistance. *Sci. Rep.* **2015**, *5* (1), 15134.
(44) Villarroel-Vicente, C.; Gutiérrez-Palomo, S.; Ferri, J.; Cortes, D.; Cabedo, N. Natural products and analogs as preventive agents for metabolic syndrome via peroxisome proliferator-activated receptors: An overview. *Eur. J. Med. Chem.* **2021**, *221*, 113535.
(45) Kaserer, T.; Obermoser, V.; Weninger, A.; Gust, R.; Schuster, D. Evaluation of selected 3D virtual screening tools for the prospective identification of peroxisome proliferator-activated receptor (PPAR) $\gamma$ partial agonists. *Eur. J. Med. Chem.* **2016**, *124*, 49−62.




https://doi.org/10.1021/acs.jafc.2c08169
J. Agric. Food Chem. 2023, 71, 1628−1642